doi:10.1016/j.jmb.2008.12.020 J. Mol. Biol. (2009) 386, 435–450

JMB

Available online at www.sciencedirect.com

ScienceDirect

ELSEVIER

Terminal Adenosyl Transferase Activity of Posttranscriptional Regulator HuR Revealed by Confocal On-Bead Screening

Nicole-Claudia Meisner[3]*†, Martin Hintersteiner[2]†, Jan-Marcus Seifert[1], Roman Bauer[1], Roger Marc Benoit[3], Armin Widmer[3], Torsten Schindler[1], Volker Uhl[1], Michaela Lang[1], Hubert Gstach[1] and Manfred Auer[2]*

[1]*Novartis Institutes for BioMedical Research, Brunnerstrasse 59, 1230 Vienna, Austria*

[2]*University of Edinburgh, School of Biological Sciences, The King's Buildings, Michael Swann Building 3.34, Mayfield Road, Edinburgh EH9 3JR, UK*

[3]*Novartis Institutes for BioMedical Research, Novartis Campus Forum 1, 4056 Basel, Switzerland*

Received 16 September 2008; received in revised form 24 November 2008 accepted 8 December 2008 Available online 14 December 2008

Edited by J. Karn

Posttranscriptional regulation and RNA metabolism have become central topics in the understanding of mammalian gene expression and cell signalling, with the 3′ untranslated region emerging as the coordinating unit. The 3′ untranslated region trans-acting factor Hu protein R (HuR) forms a central posttranscriptional pathway node bridging between AU-rich element-mediated processes and microRNA regulation. While (m)RNA control by HuR has been extensively characterized, the molecular mode of action still remains elusive. Here we describe the identification of the first RRM3 (RNA recognition motif 3) targeted low molecular weight HuR inhibitors from a one-bead–one-compound library screen using confocal nanoscanning. A further compound characterization revealed the presence of an ATP-binding pocket within HuR RRM3, associated with enzymatic activity. Centered around a metal-ion-coordinating DxD motif, the catalytic site mediates 3′-terminal adenosyl modification of non-polyadenylated RNA substrates by HuR. These findings suggest that HuR actively contributes to RNA modification and maturation and thereby shed an entirely new light on the role of HuR in RNA metabolism.

Keywords: HuR; AU-rich; posttranscriptional regulation; CONA; screening

Introduction

Regulation of mRNA turnover, transport, and translatability by AU-rich elements (AREs) is an essential control mechanism for a large number of functionally diverse, transiently expressed genes.[1,2] Recently, evidence has been accumulating that dysregulated expression and activity of the mRNA binding protein HuR (Hu protein R), a key ARE pathway node, may be fundamentally linked to the development, progression, and prognosis of malignant diseases.[3–14] Consequently, there is increasing interest in HuR as a drug target in the recent literature.[4,15,16] Nevertheless, there is still no HuR-targeted drug in pharmaceutical drug development to the best of our knowledge. This is, at least in part, associated with the pleiotropic nature of HuR. Not only is the protein responsible for balancing half-

**Corresponding authors.* E-mail addresses: nicole-claudia.meisner@novartis.com; manfred.auer@ed.ac.uk.

† N.-C.M. and M.H. contributed equally to this work.

Abbreviations used: HuR, Hu protein R; RRM, RNA recognition motif; ARE, AU-rich element; CONA, confocal nanoscanning; AIDA, an indazole-based discovery and analysis tool; MS, mass spectrometry; IL, interleukin; NTP, nucleoside triphosphate; PAP, poly(A) polymerase; GTP, guanosine 5′-triphosphate; EDTA, ethylenediaminetetraacetic acid; CTP, cytidine triphosphate; UTP, uridine triphosphate; TNFα, tumor necrosis factor-α; UTR, untranslated region; WT, wild type; PBS, phosphate-buffered saline.

0022-2836/$ - see front matter © 2009 Published by Elsevier Ltd.

lives, localization, and translatability of functionally diverse ARE mRNAs;[17,18] recently, HuR has even been linked to microRNA pathways.[19] Hence, its ultimate validation as a drug target still remains an open call.

For validating drug targets, gene silencing induced by small interfering RNA has greatly facilitated the characterization of gene function. However, a depletion of the gene product may not necessarily translate to a functional inhibition of the protein in a therapeutic situation.[20–22] A full assessment of the benefits and risks associated with therapeutic HuR inhibition will therefore require functional inhibition or modulation by small-molecule inhibitors. Recently, we described MS-444, dehydromutactin, and okicenone as the first low molecular weight inhibitors for HuR.[23] Whilst these natural products present great tools to characterize the phenotypic consequences of HuR inhibition, additional compound classes of different mechanisms and chemotypes will be of strategic importance for dissecting on-target from off-target effects and for studying different HuR activities in an uncoupled fashion. In fact, the modular domain organization of this RRM (RNA recognition motif) protein together with an increasing number of reports that are unravelling new HuR interaction partners[9,24–29] suggests the existence of multiple functional sites associated with different activities. The previously identified compounds MS-444, okicenone, and dehydromutactin target a site within RRM1 and RRM2, which is the best characterized and most conserved part across Hu family members, associated with HuR homodimerization[23,26] and binding to ARE RNA (NNUUNNUUU).[30–33] In contrast, the contribution of the C-terminal hinge and RRM3 domain to HuR's mode of action remains rather unclear. On one hand, there is still a lack of information on the structure of this part of the protein as well as on the nature and motif of any putative RNA ligand for RRM3. On the other hand, the key to our understanding of how HuR orchestrates multiple cellular programs[3,17] appears to be inherently linked to a mechanistic characterization of the C-terminal domain(s). Not only is this the region that differentiates HuR most from the other Hu proteins, but residues within the C-terminal part of HuR have been implicated in a number of processes beyond RNA binding such as nucleocytoplasmic shuttling,[34,35] recognition of protein ligands,[25,36] as well as posttranslational methylation,[37] phosphorylation,[24,29] or caspase cleavage.[26] To cover putative drugable pockets associated with these functions of the hinge/RRM3 region, affinity-based compound screening, specifically on-bead,[38,39] represents an efficient and fast approach to identify small-molecule ligands and tools.

Here we describe the identification of RRM3-targeted low molecular weight ligands from a differential confocal nanoscanning (CONA) on-bead screen of full-length HuR *versus* HuR_{12} (encompassing RRM1 and 2 only). A mechanistic characterization revealed that ATP is a natural ligand for this orphan binding pocket, which is centred on a classical and functionally conserved Me^{2+}-binding DxD motif. Finally, we demonstrate that HuR functions as an RNA-modifying enzyme, using the ATP-binding DxD cleft for non-templated 3′-terminal adenosyl transferase activity.

Results

A differential CONA on-bead screen identifies RRM3-targeted small-molecule HuR ligands

In the search for small-molecule ligands targeting orphan binding pockets within the C-terminal domain(s) of HuR, we performed a differential on-bead screen with full-length HuR *versus* HuR_{12} (Fig. 1). From a stock library of 2.2 Mio bead immobilized heterocyclic compounds, a representative, diversity-optimized subset of 89,000 compounds ("master plate")‡ was screened by CONA (confocal nanoscanning/bead picking).[41] CONA represents a high-resolution, high-speed and quantitative technology for high-throughput screening of one-bead–one-compound libraries. In CONA, the confocal detection volume is used to scan a layer of library beads in a microtiter plate to generate a cross-section image at the equatorial plane of the beads (Fig. 1b and c); thereby, binding of fluorescently labelled proteins to cognate compounds on the bead surface is detected as a fluorescent ring, with an intensity proportional to the amount of bound protein. From the different scaffold classes comprised in the master plate compound selection, full-length HuR selective hits with exceptionally bright rings were found in the sublibraries containing pyrrole and dicarboxylic acid scaffolds (Fig. 1a). Forty-six structures were elucidated by mass spectrometry (MS) decoding of the material derived from isolated hit beads. Among the decoded hits, a preference for specific building blocks was observed in most combinatorial positions (Fig. 2a). Moreover, four individual structures were found repetitively (one fivefold and three duplicate hits, Fig. 2b). These compounds were resynthesized at a larger scale with (**1**, **3**, **5**, **7**) and without the AIDA tag (an indazole-based discovery and analysis tool[40]) (**2**, **4**, **6**, **8**), which is built into every compound of the primary screening libraries. To confirm the initial screening hits and exclude any potential influence of the AIDA tag, resins with both tagged and untagged compound variants were rescreened with full-length HuR *versus* HuR_{12} using unlabelled protein and fluorescent antibody detection (on-bead confirmation). As expected, none of the resin-bound compounds showed binding of HuR_{12}, while association with full-length HuR was confirmed for the compound pairs H1A **1**/H1N **2**, H2A **3**/H2N **4**, and

‡ A CONA masterplate comprises 89,000 compounds (i.e. beads) representative for the entire screening collection (2.2 Mio compounds) which are compiled in one 96well microtiter plate, whereas sublibraries with different heterocyclic scaffolds are distributed into individual wells.

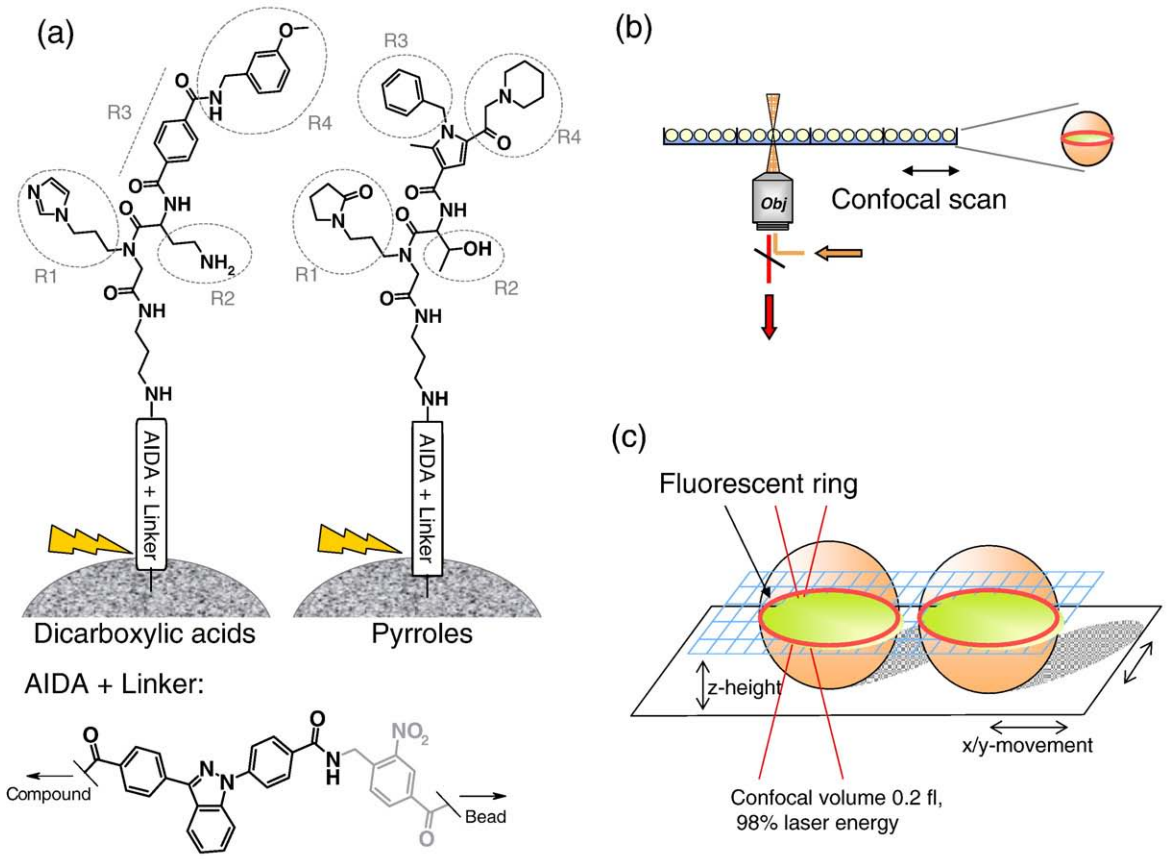

Fig. 1. Confocal on-bead screening (CONA) and library design. (a) One-bead–one-compound libraries of different heterocyclic scaffolds were synthesized by a split–mix–divide procedure. Each compound class comprises four combinatorial positions, which are shown for two exemplary sublibraries of the dicarboxylic acid and pyrrole series. As the beads are kept separate after the third combinatorial coupling step, the building blocks in R3 and R4 define the library and sublibrary, respectively. All libraries were synthesized on a photosensitive nitrobenzyl linker (shown in grey). In addition, the chemical setup contains a generic (UV-excitable fluorescent) decoding and analysis tag (AIDA[40]) that is spaced from the compounds by a three-carbon atom diamine linker. (b) For CONA screening, 1 mg resin (~2000 beads) from individual sublibraries are distributed into different wells of a 96-well microtiter plate to form a monolayer at the well bottom. After incubation with low nM concentrations of a fluorescently labelled target protein, the beads are screened by large-area confocal scanning to detect protein binding to the compounds at the outer layer of the beads. (c) The confocal scan generates an *x*–*y* cross-section image slightly below the equatorial plane of the beads. Binding of fluorescently labelled protein to a bead-immobilized compound is detected as a fluorescent ring and quantified based on the fluorescence intensity at the outermost layer of the beads (~5 μm). A software-based analysis of the images allows to determine the *x*–*y* coordinates of each individual bead. The spatial fluorescence intensity profile allows to exclude autofluorescent beads. Hit beads are isolated via a semi-automated capillary picking system. As the fluorescence ring intensity is proportional to the amount of bound protein, CONA inherently provides a quantitative method for target–ligand interactions on bead.

H3A **5**/H3N **6** (Fig. 2c). On-bead confirmation for the resins H4A **7** and H4N **8** was negative or weakly positive, respectively. Due to the orphan nature of the targeted binding pocket, it is inherent that no functional or biochemical assay was available to assess the compounds' potency in solution. Generally, the AIDA tag provides an intrinsic UV-excitable tracer for target protein interactions in solution. However, the AIDA-tagged variants of the HuR hit compounds were highly hydrophobic, which impaired any measurements with the tagged compounds at physiological buffer conditions. Nevertheless, the ability of quantitative detection of on-bead binding with CONA provided an additional assay for the newly identified ligand site. Binding of HuR to the best on-bead resin (H1N) was quantitatively determined in the presence and absence of the (non-AIDA) compounds in solution (Fig. 2d). Indeed, the fivefold replicate hit (H1N, in solution) significantly reduced the amount of HuR bound to the H1N-resin, while we did not observe any competition for the less potent compounds H2N, H3N, and H4N at their highest possible concentration. It is, however, noteworthy to mention that due to the high local compound density on-bead (concentrations in the millimolar range), a high affinity and/or concentration of the competitor in solution is required to detect a significant competitive reduction of on-bead binding (simulation data not shown). Based on the on-bead confirmation and competition

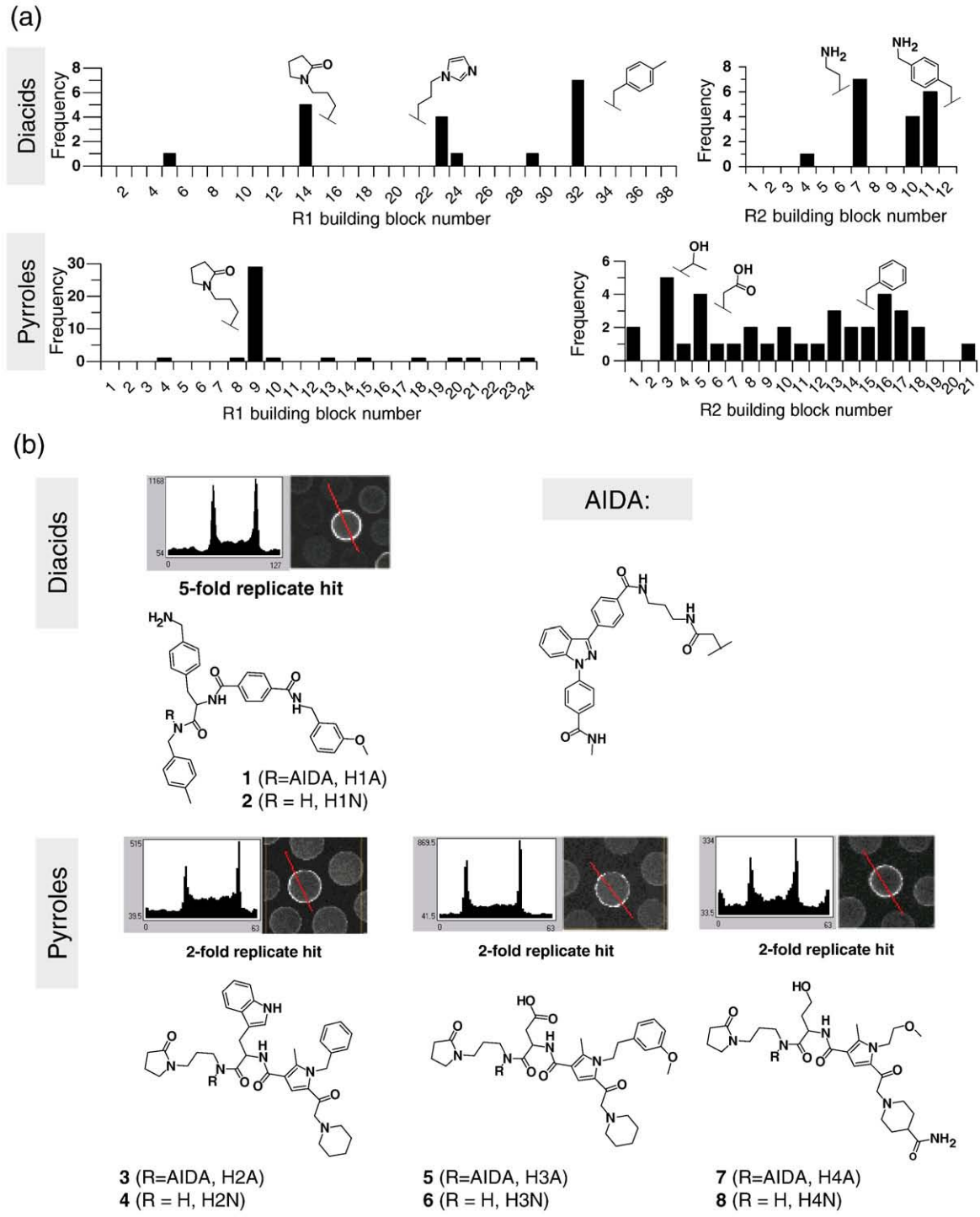

Fig. 2. Small-molecule HuR ligands identified by CONA — primary screening and confirmation. (a) The hit compound structures were revealed by MS after photolytical cleavage of the compounds from the beads. Full-length HuR selective hits with highest ring intensities were found in sublibraries of two scaffolds (dicarboxylic acids and pyrroles; see Fig. 1a). The frequency of building blocks in the combinatorial positions R1 and R2 of the decoded hit structures is shown for each of the two scaffolds. (b) Four structures were found repetitively and resynthesized individually, with and without the AIDA tracer and the 3-aminopropane linker. Primary CONA screening images of one representative hit bead of each replicate hit are shown together with the fluorescence intensity profile (kilohertz; cross-section indicated by a red line). (c) Confirmation of resynthesized CONA hits: resynthesized compounds on the resins were tested to confirm on-bead binding of full-length HuR *versus* HuR_{12} (CONA images; unlabelled protein at 200 nM, with antibody detection). (d) The quantitative on-bead binding assay was used to assess the resynthesized compounds' activity in solution. Binding of full-length HuR to the H1N resin was quantified by CONA in the presence of different competitors in solution [ARE IL-1β RNA at 10 μM, H1N–H4N at 100 μM each, MS-444 at 10 μM, dimethyl sulfoxide in all samples at 2.5% (v/v)]. Data points represent fluorescence ring intensities averaged over 100 beads, ±SD, and are representative for at least two independent experiments.

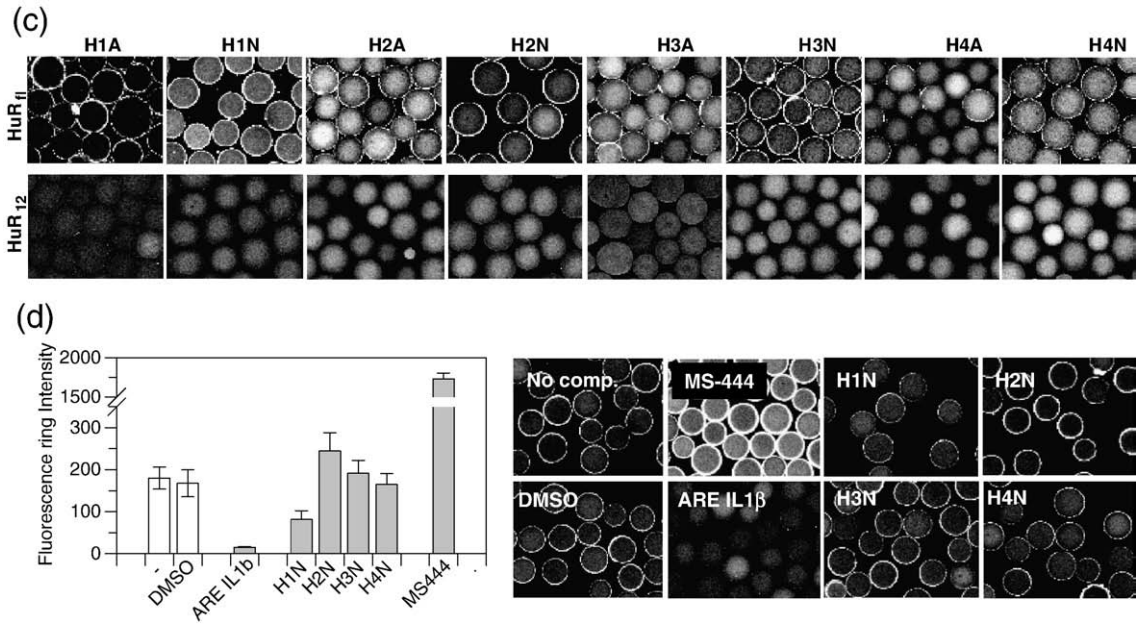

Fig. 2 (*legend on previous page*)

data, we focused on the most potent compound H1N for all further characterization studies.

CONA compound characterization reveals an ATP-binding pocket within RRM3

To further characterize the effect of the identified compounds on known HuR activities, we tested H1N for inhibition of ARE RNA binding and HuR homodimerization, both functions being exerted by RRM domains 1 and 2.[23,30–33] As expected, the C-terminus targeted compound H1N did not interfere with HuR homodimerization (Supplementary Online Material). However, a weak inhibition of complex formation between full-length HuR and an RNA encompassing the ARE region of interleukin (IL) 1β mRNA in solution was observed (Supplementary Online Material). *Vice versa*, the same 33-mer RNA inhibited binding of HuR_{fl} to resin-bound compound H1N (Fig. 2d). In consistence with the assignment of the CONA compounds to the C-terminal hinge or RRM3 domain, H1N did not interfere with solution binding of HuR_{12} to the same RNA (Supplementary Online Material). With ARE RNA binding being assigned primarily to RRM1+2 and the CONA compound binding site mapping to the C-terminal domains, there are two conceivable explanations for the observed mutual inhibition. One possible explanation might be an allosteric coupling of the two binding pockets. Alternatively, the ARE RNA might contact additional amino acids in RRM3 within a region shared with the CONA ligands. Interestingly, the dimerization inhibitor MS-444 dramatically enhanced on-bead binding of full-length HuR to the H1N resin, indicating an optimized steric conformation or accessibility of the CONA compound binding pocket in the HuR monomer.

Having identified small molecules directed to the C-terminus of HuR, the question arose as to whether these compounds hit a truly orphan binding site or mimick a natural ligand. Interestingly, we had previously observed that full-length HuR, but not HuR_{12}, reacted highly sensitively to divalent cations and precipitates in the presence of low millimolar concentrations of Zn^{2+}, Ca^{2+}, or Co^{2+}, but is stable under conditions of Mg^{2} or Mn^{2}. Therefore, we analyzed the HuR sequence for known metal-ion-binding motifs. Indeed, within RRM3 there is a canonical DxD motif that is functionally conserved across Hu family members and species (Supplementary Online Material). This class of Me^{2+} ion coordinating motifs is commonly used for recognition of nucleoside triphosphate (NTP) and related cofactors in proteins such as glycosyl transferases,[42] CCA-adding enzymes,[43] as well as poly(A) polymerase (PAP)[44] or other Pol-β nucleotidyl transferases.[45,46] Therefore, we tested whether NTPs compete with the CONA compounds for binding to HuR. Consistent with a hypothesized related relevance of DxD in HuR, binding of HuR to the H1N resin was substantially reduced in the presence of both NTPs and deoxynucleoside triphosphates (dNTPs) (Fig. 3a). While guanosine 5′-triphosphate (GTP) showed the lowest degree of inhibition, generally no pronounced selectivity for either nucleotide was observed. A direct HuR–NTP interaction was further confirmed by the binding of full-length HuR (but not HuR_{12}) to bead-immobilized ATP (Fig. 3b). Again, the addition of an excess of ATP in solution reduced the levels of HuR–ATP complex formation on-bead. Considering that ATP and GTP are the physiologically prevalent NTP cofactors, we measured binding of fluorescently labelled ATP *versus* GTP to HuR in an ELISA setup as an orthogonal method to the on-bead

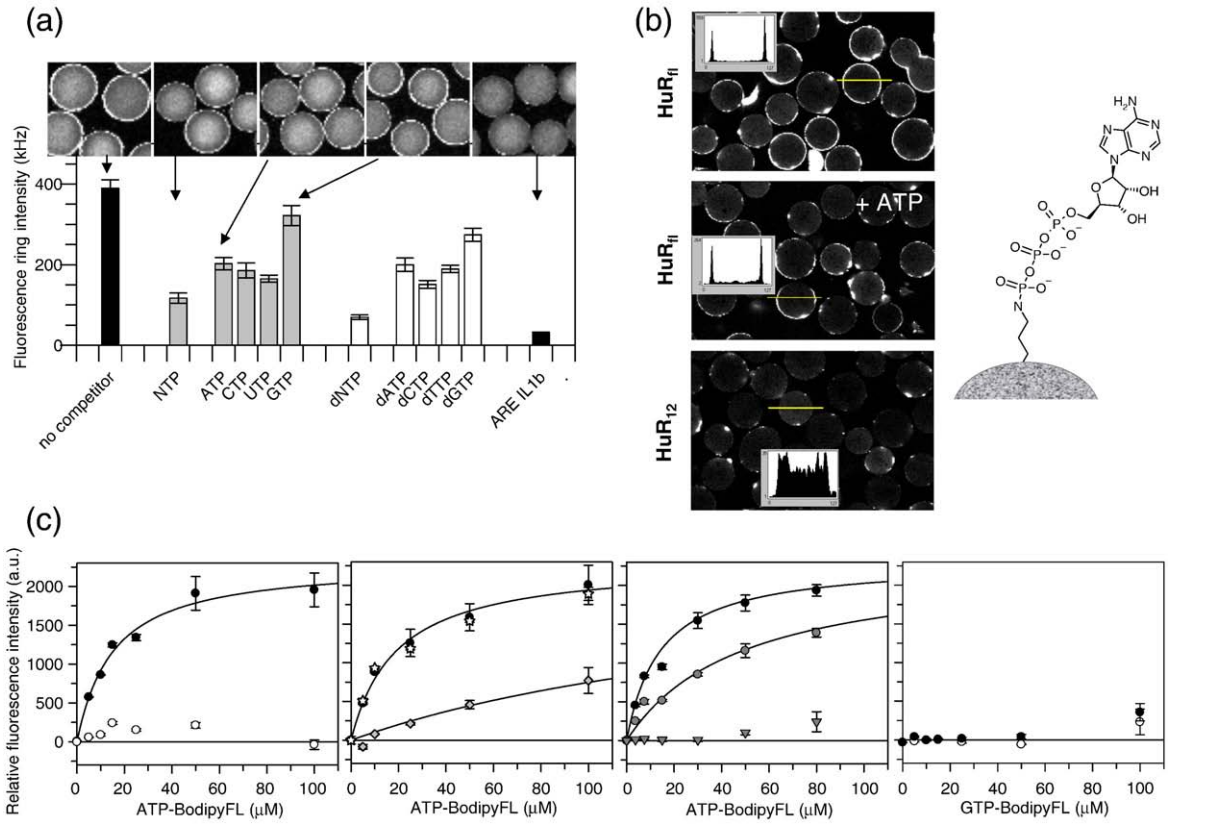

Fig. 3. Identification of ATP as HuR RRM3 ligand. (a) Binding of full-length HuR (at 200 nM, with fluorescent antibody detection) to the H1N resin was quantitatively measured by CONA in the presence of NTP or dNTP mixes (each nucleotide at 5 mM) or individual nucleotides (at 5 mM). Competition with ARE IL-1β RNA (at 10 μM) is shown as positive control. Data points represent fluorescence ring intensities (kilohertz) averaged over 100 beads ±SD and are representative for at least two independent experiments. (b) Binding of full-length HuR *versus* HuR_{12} to bead-immobilized ATP detected with CONA. A competition with 5 mM ATP in solution is shown in the middle image, the ATP–bead linkage chemistry is shown in the right panel. Representative fluorescence intensity profiles are shown as inset (cross-section indicated by yellow line). (c) Binding of 5′-Bodipy FL-labelled ATP or GTP to full-length HuR *versus* HuR_{12} was measured in an ELISA setup. After incubation with recombinant HuR (or HuR_{12}, both at 750 nM) in solution, complexes were captured to the surface-immobilized anti-HuR antibody (19F12) and bound ATP or GTP was quantified by Bodipy FL fluorescence ($MgCl_2$ at 10 mM in all samples). Data represent averages±SD of five independent samples and are representative for at least three independent experiments. First panel: Binding of ATP-Bodipy FL to HuR_{fl} (black dots, $K_{d(ATP)} = 14.3 \pm 2.3$ μM) *versus* HuR_{12} (white dots). Second panel: Binding of ATP-Bodipy FL to HuR_{fl} in the absence (black dots, $K_{d(ATP)} = 14.9 \pm 2.9$ μM) and presence of ARE IL-1β RNA (10 μM, white stars, $K_{d(ATP)} = 15.6 \pm 3.1$ μM) or EDTA (10 mM, grey dots, $K_{d(ATP)} = 208 \pm 22$ μM). Third panel: Binding of ATP-Bodipy FL to HuR_{fl} in the absence (black dots, $K_{d(ATP)} = 14.1 \pm 1.2$ μM) and presence of H1N (100 μM, grey dots, $K_{d(H1N)} = 45 \pm 6$ μM based on a nonlinear fit for a 1:1 competitive inhibition) or MS-444 (20 μM, grey triangles). Fourth panel: Titration of HuR_{fl} (black dots) *versus* HuR_{12} (white dots) with GTP-Bodipy FL.

assay§. No interaction of GTP with HuR_{12} or HuR_{fl} was observed, whereas ATP bound selectively to full-length HuR with an affinity of $K_d = 15 \pm 3$ μM (Fig. 3c). A metal ion dependence of the HuR ATP interaction was supported by the reduced affinity in the presence of stoichiometric concentrations of ethylenediaminetetraacetic acid (EDTA) ($K_d = 210 \pm 20$ μM). No mutual interference between binding of ATP and an ARE RNA (IL-1β) to HuR was detected (Fig. 3c and Supporting Online Material), whereas disruption of the HuR dimer by MS-444 was accompanied by an impaired HuR ATP recognition (Fig. 3c). Eventually, the ATP–HuR interaction provided a solution assay for testing and quantifying direct competition of H1N with the putative natural ligand. As the inhibition data were compatible with a 1:1 competition model [K_d (H1N) = 45±6 μM], this supported a shared binding site between the newly identified RRM3 ligands H1N and ATP.

§ Due to the low solubility of full-length HuR (ca. 1 μM), the 15μM K_d interaction with ATP could not be measured under equilibrium conditions in homogeneous solution.

HuR is an RNA-modifying enzyme with 3′-terminal adenosyl transferase activity

There are several conceivable roles for ATP as a newly identified HuR cofactor. The two general

mechanistic possibilities comprise either functions where ATP hydrolysis serves as an energy source (e.g., for conformational changes or helicase activities) or where ATP is used as cofactor for enzymatic modification of a (most likely RNA) substrate. As a starting point, we therefore tested a potential substrate-independent hydrolysis of ATP by HuR.

Radiolabelled ATP ([α-^{33}P]ATP) was treated with full-length HuR, HuR_{12}, calf intestinal phosphatase, or PAP and separated from potential dephosphorylated products by thin-layer chromatography. In contrast to calf intestinal phosphatase, neither full-length HuR nor HuR_{12} (nor PAP) showed any increase in the relative ADP and/or AMP levels (Fig. 4a). In the absence of structural information on HuR, we resorted to a homology model of RRM3 to get hints on the global positioning of the DxD motif in relation to the RNA binding surface (Figs. 7a and b). Protein Data Bank (PDB) structures that were most similar to the predicted RRM3 fold were superimposed to identify a consensus region. Five structures representative for the consensus were selected (RRM1 of HuC, RBD3 of CUG triplet repeat RNA-binding protein 1, ATP-binding domain of DEAD-box helicase, RRM1 of Sex-lethal, BPTI domain of bovine trypsin inhibitor) and used to generate a combined template for homology modelling. Interestingly, the RRM3 model suggests that the DxD motif (D_{254}, D_{256}) is solvent exposed and is located in immediate proximity to an extended, shallow, and positively charged groove, the presumptive RNA binding surface of RRM3. This configuration intuitively suggests an RNA-modifying, e.g., transferase, or polymerase activity for RRM3. Hence, we used total RNA from mammalian cells as substitute for the unknown RNA substrate to test a potential incorporation of α-^{33}P-

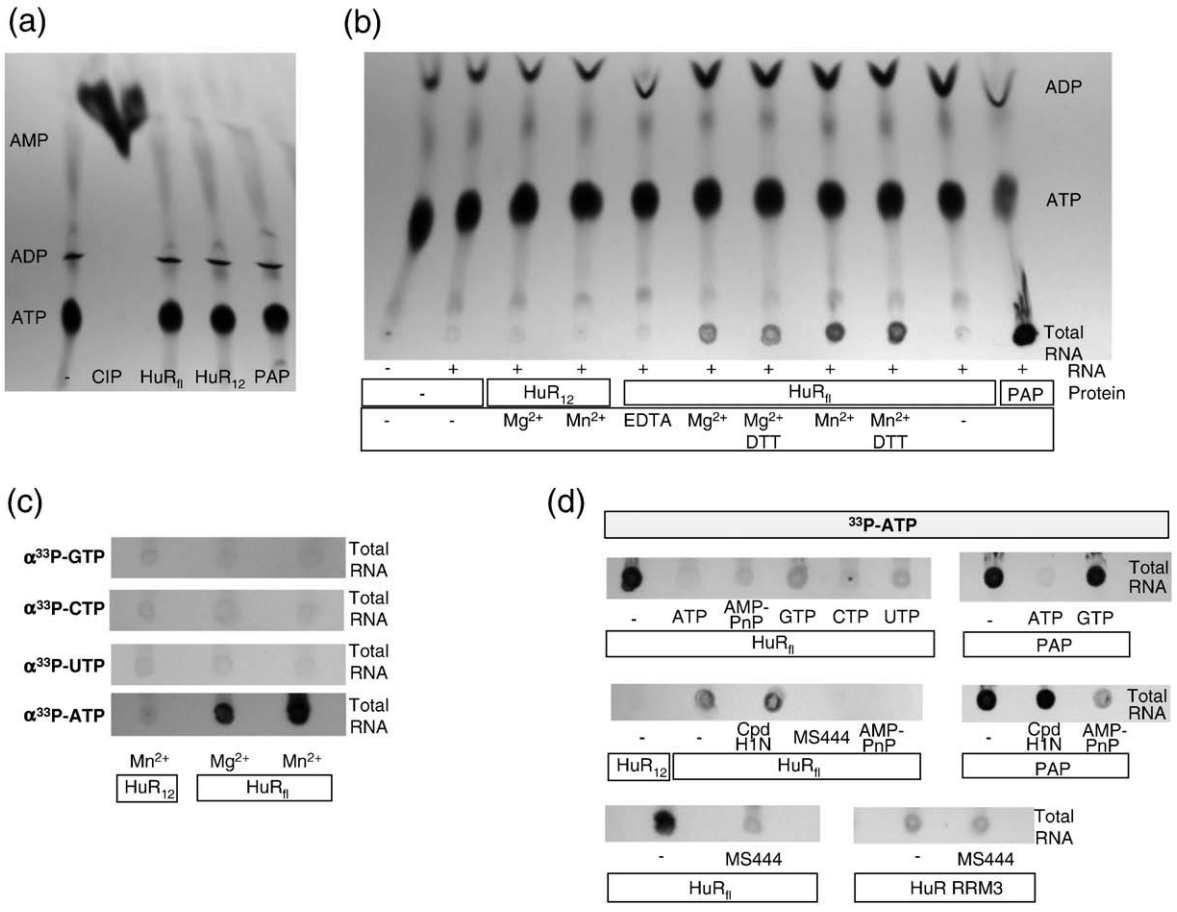

Fig. 4. Functional relevance of the HuR ATP-binding site. (a) Hydrolysis of α-^{33}P-labelled ATP (2 μCi, 330 nM) after protein treatment was analyzed by thin-layer chromatography and autoradiography to visualize ATP, ADP, and AMP. [α-^{33}P]ATP only (lane 1) or after incubation with calf intestinal phosphatase (5 U, lane 2), HuR_{fl} (750 nM, lane 3), HuR_{12} (750 nM, lane 4) or *E. coli* poly(A) polymerase (4 U, lane 5). (b) To monitor incorporation of adenosyl into RNA, α-^{33}P-labelled ATP (330 nM) was incubated with or without full-length HuR *versus* HuR_{12} (each at 750 nM) and total RNA from HEK293T cells (1 μg) under different metal ion or buffer conditions ($MgCl_2$ at 10 mM, $MnCl_2$ at 1 mM, DTT at 1 mM) and separated by thin-layer chromatography. Incorporated radioactive adenosyl accumulated together with bulk RNA in the base spot and was visualized by autoradiography. Poly(A) polymerase (4 U) was used as positive control. (c) Incorporation of radiolabelled (α-^{33}P) nucleotides (each at 2 μCi, 330 nM) into total RNA (2 μg) by full-length HuR *versus* HuR_{12} (each at 750 nM) was monitored by thin-layer chromatography and autoradiography of the bulk RNA (only base spots shown). (d) Incorporation of α-^{33}P-labelled adenosyl (330 nM) into total RNA (2 μg) by full-length HuR *versus* HuR_{12} and RRM3 (each at 750 nM) in the presence of different competitors as indicated (all NTPs at 5 mM, H1N at 50 μM, MS-444 at 50 μM; all samples with 1 mM $MnCl_2$). Data are representative for at least three independent experiments.

radiolabelled adenylate, monitored by thin-layer chromatography. As any RNA accumulates in the base spot, this method is ideally suited to monitor bulk RNA without separation into individual species. Indeed, an incorporation of radiolabelled adenylate into total RNA by HuR_{fl} was observed (Fig. 4b). The inactivity of HuR_{12} supported the essential role of RRM3. As reported for most other DxD enzymes, the activity was strongly dependent on the presence of divalent cations ($Mn^{2+} > Mg^{2+}$), and also inhibited by chelation of metal ions with EDTA. Consistent with the negative HuR binding results for GTP (Fig. 3c) no RNA modification with radiolabelled GTP was observed (Fig. 4c). Also, a competition of nonisotopic NTPs with [α-^{33}P]ATP incorporation reproduced the relative NTP activities as detected in the CONA on-bead competition assay with H1N [(ATP ~ CTP ~ UTP)>GTP, Fig. 4d]. Interestingly, although ATP, cytidine triphosphate (CTP) and uridine triphosphate (UTP) displayed comparable binding activities (Figs. 3a and 4d), the enzymatic activity showed a strong selectivity for incorporation of adenosine (Fig. 4c). Based on a comparison to *Escherichia coli* PAP (Fig. 4b), HuR appears to be a relatively slow enzyme under the applied experimental conditions. However, this might of course be limited by the putatively low concentration of the fraction of suitable substrates in the total RNA population or by the lack of additional, as yet unidentified cofactors. To rule out the possibility that the observed enzymatic function might be influenced by traces of contaminating *E. coli* enzymes, the previously identified HuR dimerization inhibitor MS-444 was used as an independent control. Consistent with the HuR ATP-binding data (Fig. 3c), the transferase reaction was inhibited by MS-444 (Fig. 4d). Together with the inactivity of HuR_{12} purified following an identical procedure, this unambiguously relates the observed adenosyl incorporation to HuR. A markedly lower yet residual transferase activity was detected for the isolated RRM3 domain (as fusion protein with mCherry), which was not sensitive to the RRM1+2-associated compound MS-444 (Fig. 4d).

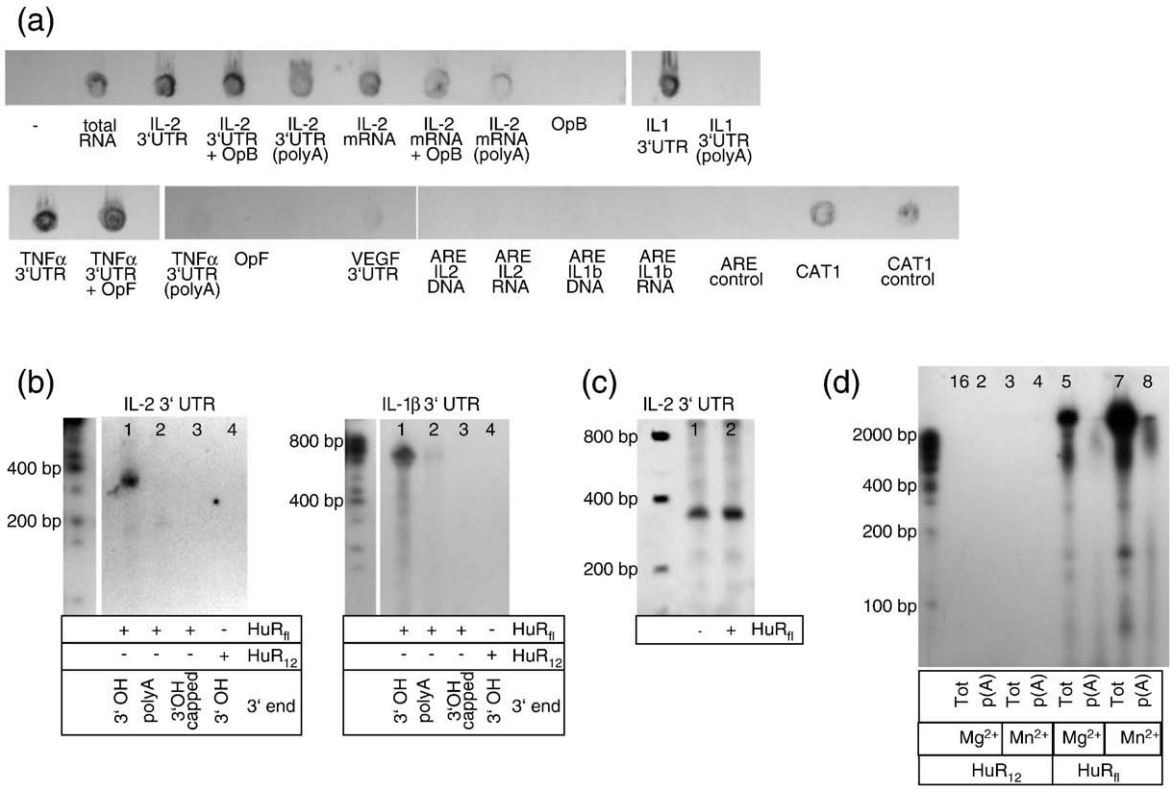

Fig. 5. 3′-Terminal RNA modification by the adenosyl transferase activity of HuR. (a) Incorporation of α-^{33}P-labelled adenosyl (ATP, at 330 nM) into different RNA substrates as indicated (all RNA samples at 1 μM, HuR_{fl} at 750 nM, $MnCl_2$ at 1 mM), monitored by thin-layer chromatography and autoradiographic detection (only base spots with the adsorbed RNA are shown). OpB, IL-2 opener B; OpF, TNFα opener F (both from Ref. 31); ARE, AU-rich element; poly(A), *in vitro* pre-polyadenylated RNA as indicated. (b) IL-2 and IL-1β 3′UTR fragments (281 and 594 nt, respectively; 25 pmol each) were treated with HuR_{fl} or HuR_{12} (each at 750 nM) and [α-^{32}P]ATP (330 nM) and analyzed by PAGE with autoradiographic detection. Size standard: low DNA mass ladder (5′-phosphorylated with [γ-^{32}P]ATP), HuR_{fl} treated RNA with a free 3′-OH (lane 1), a poly(A)-tail (lane 2) or a capped 3′-OH (lane 3, with Cy3). HuR_{12}-treated RNA (free 3′-OH) is shown in lane 4. (c) PAGE analysis and ethidium bromide staining of an IL-2 3′UTR fragment (25 pmol, 281 nt) before (lane1) and after (lane 2) reaction with HuR_{fl} (750 nM) and ATP (1 mM). Size standard: low DNA mass ladder. (d) Total RNA (Tot, 13.5 μg) or poly(A) RNA [p(A), 0.15 μg] from HEK293T cells (both from an equivalent number of cells) was treated with HuR_{fl} or HuR_{12} (each at 750 nM) and [α-^{32}P]ATP (330 nM) in the presence of $MgCl_2$ (10 mM) or $MnCl_2$ (1 mM) and analyzed by PAGE with autoradiographic detection. Size standard: low DNA mass ladder (lane 1, 5′-phosphorylated with [γ-^{32}P]ATP).

Compound H1N did not significantly reduce the amount of incorporated radioactivity at a compound concentration of 50 μM (Fig. 4d), most likely due to the low affinity (K_d = 45 μM) of the compound.

To further elucidate the potential nature of the RNA substrate(s), we tested the HuR adenosyl transferase activity for a selection of 3′ untranslated region (UTR) fragments from HuR target mRNAs containing or missing the RRM1+2 binding motif, NNUUNNUUU (Fig. 5a). While NNUUNNUUU-containing fragments of the IL-2, IL-1β, tumor necrosis factor-α (TNFα) and CAT1 mRNAs proved to be cognate substrates, an ARE (and NNUUNNUUU) deletion construct of the CAT1 mRNA fragment showed no markedly reduced incorporation. *Vice versa*, fragments encompassing the ARE only (IL-2, IL-1β) were poor substrates. As the suitability of RNA substrates for the HuR adenosyl transferase activity was hence apparently unrelated to the previously established criteria for RNA recognition by RRM1+2 ,[31,49,50] we analyzed the HuR-treated total RNA by PAGE to obtain an impression of the size distribution of preferred RNA substrates (Fig. 5d). Distinct radiolabelled bands appeared across the entire size range, whereas the bulk substrate population clustered at a size of 800 nucleotides or longer. Interestingly, an equivalent amount of the poly(A) subset of the isolated total RNA showed a largely reduced nucleotide incorporation. Further supporting this observation, an *in vitro* pre-polyadenylation of the IL-2, IL-1β, and TNFα mRNA 3′UTR fragments markedly reduced or abolished further adenosyl addition by HuR (Fig. 5a).

To reveal whether the modification indeed occurs at the RNA 3′ terminus, we monitored different variants of selected RNA substrate after HuR treatment by PAGE. For IL-2 and IL-1β mRNA substrates containing a free 3′-OH, a radiolabelled band appeared at the length of the original substrate after reaction with full-length HuR but not HuR_{12} (Fig. 5b). A visualization by ethidium bromide staining showed that the RNA was not significantly elongated after reaction with HuR and ATP, suggesting that only one or a few nucleotides are incorporated and no long homopolymeric tails are synthesized (Fig. 5c). The PAGE analysis also confirmed that an *in vitro* pre-polyadenylation of the RNA substrates inhibited a further enzymatic modification by HuR (Fig. 5b). Moreover, capping of the 3′-OH (Cy3 hydrazide) abolished any adenosyl incorporation by HuR (Fig. 5b), underlining the requirement of a free 3′-OH as acceptor group for modification.

A metal-ion-binding DxD motif is an essential element of the HuR catalytic site

As both the homology model as well as the experimental data on the metal ion dependence of the RRM3 adenosyl transferase activity supported a direct contribution of the DxD motif, we generated HuR point mutants. In many DxD enzymes, a third acidic side chain is found in the immediate vicinity

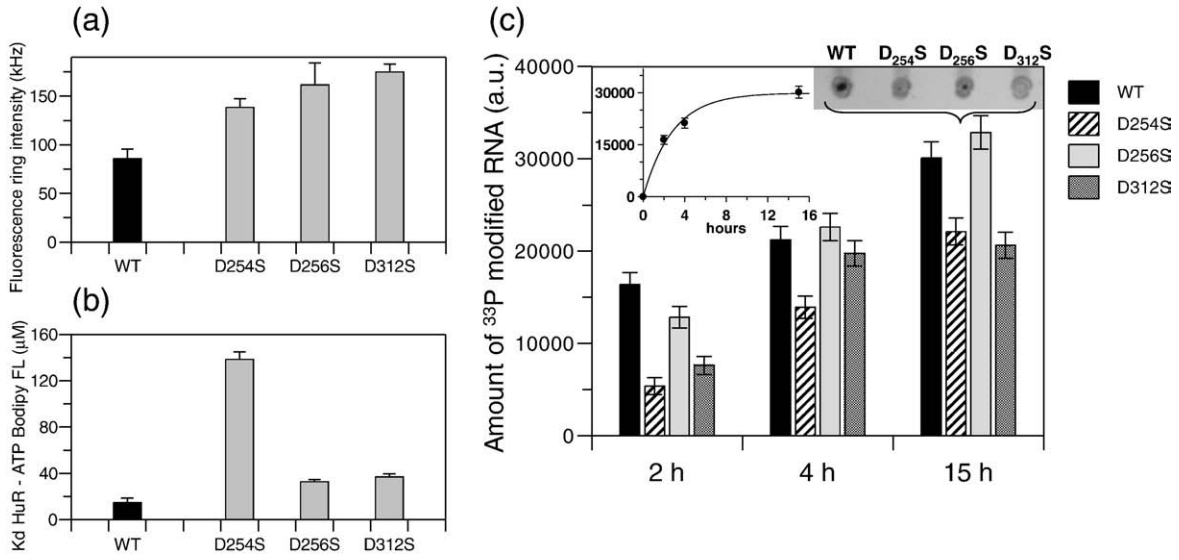

Fig. 6. Characterization of ATP-binding site by HuR DxD mutants. (a) Quantification of binding of WT *versus* mutant HuR_{fl} (as indicated) to the H1N resin was quantitatively measured by CONA (all proteins unlabelled and at 70 nM, with fluorescent antibody detection). Data points represent fluorescence ring intensities averaged over 100 beads, ±SD, and are representative for at least two independent experiments. (b) Binding affinities of 5′-Bodipy FL-labelled ATP to WT *versus* mutant HuR_{fl} (as indicated) as determined by the ELISA assay (all proteins at 70 nM). Data represent averages ±SD of five independent samples and are representative for at least two independent experiments. (WT: $K_{d(ATP)}$ = 15±4 μM, $D_{254}S$: $K_{d(ATP)}$ = 140±10 μM, $D_{256}S$: $K_{d(ATP)}$ = 33±2 μM, $D_{312}S$: $K_{d(ATP)}$ = 37±3 μM). (c) Incorporation of α-^{33}P-radiolabelled ATP (330 nM) into total RNA (1 μg) after 2 , 4 , and 15 h incubation with WT *versus* mutant HuR_{fl} (as indicated; all proteins at 70 nM) was quantified by thin-layer chromatography with autoradiographic detection. The time course of the reaction is shown for the WT protein in the inset. Data represent total autoradiographic density in the RNA spot after background correction, SD denotes standard deviation of the detection method as determined from a separate experiment.

of the two aspartates to surround the active site. Also in HuR there is an additional surface-exposed aspartate (D_{312}) that faces the $D_{254}xD_{256}$ motif according to the RRM3 model. Due to the low solubility of full-length HuR associated with the high hydrophobicity of the C-terminal region, we generated D→S (rather than D→A) mutants of D_{254}, D_{256}, and D_{312}. A functional characterization confirmed that all three mutants retained unchanged RRM1+2-mediated activities, with identical ARE RNA binding affinities and homodimerization activities as compared to that of the wild-type (WT) protein (Supplementary Online Material). Interestingly, the on-bead assay revealed an increased affinity of the mutants to the CONA compound H1N with an activity of $D_{312}>D_{256}>D_{254}>$WT (Fig. 6a). In ATP binding, a particular role became apparent for D_{254}. While the other two aspartate mutants D_{256}S and D_{312}S showed only 2-fold-reduced ATP binding affinities, a ~10-fold reduction in affinity was measured for the D_{254}S mutant in the ELISA assay [K_d(WT) = 15±3 μM; K_d(D_{254}S) = 140± 10 μM; K_d(D_{256}S) = 33±2 μM, K_d(D_{312}S) = 37±3 μM; Fig. 6b and Supporting Online Material]. The impact on the transferase reaction was approximately equal for the D_{254}S or D_{312}S mutants (67% or 54% reduction in ATP incorporation after 2 h incubation, respectively; Fig. 6c), whereas a mutation of D_{256} to serine showed no strong influence. These data suggest that D_{254} and D_{312} are directly involved in the catalysis, where D_{254} is a key residue for ATP binding and D_{312} plays a role in RNA substrate complexation. The contribution of D_{256} was not evident from the experiments with the D→S mutants, and might likely only be revealed by a mutation to a more dissimilar amino acid side chain. In addition, the general reduction in catalytic activity for the D_{254}S and D_{312}S mutants was not dramatic (≤60%) and can most likely be attributed to the retained H-bonding propensity of serine. Even stronger effects should be expected for double mutants or exchanges to more dissimilar (e.g., D→A) amino acids, however, these alterations will likely increase the already high hydrophobicity and aggregation tendency of full-length HuR.

As the CONA-derived HuR ligand H1N interfered with ATP as well as RNA binding, this further supports that the two interactions map to adjacent sites and that the compound binding pocket overlaps with both regions. Potential compound and ATP binding modes as suggested by docking computations with the homology model are illustrated in Fig. 7a and b (and in the Supporting Online Material). Consistent with the relatively large size of both classes of the CONA-derived HuR ligands (dicarboxylic acids, pyrroles), the hypothetical binding mode extends over the $D_{254}xD_{256}$ ATP binding hot spot into the positively charged, putative RNA substrate-binding cleft. The fact that MS-444 treatment inhibits ATP but enhances H1N binding suggests that dimer disruption results in a major conformational change that largely affects the extended, multifeatured binding pocket in RRM3. While these interaction modes are certainly limited by the validity of the homology model as well as the computational docking approach, the suggested overall compound positioning is further supported by the primary screening data. In particular, the hits in the dicarboxylic acid diamide library showed a preference for primary amines and H-bond acceptors at combinatorial position R2 (Fig. 2a), which would be explained by the suggested salt bridge interaction of R2 in H1N with aspartate D_{254} (Fig. 7b). Likewise, the pyrrole hits clustered around sublibraries with a basic nitrogen-containing building block in combinatorial position R4, the putative D_{254} contacting moiety of the docked pyrrole compounds (Supporting Online Material).

Discussion

We describe the identification of a new class of low molecular weight HuR ligands and their use for discovering a so far undescribed enzymatic activity of HuR that is exerted by RRM3. Using the quantitative CONA on-bead screening method, we were able to obtain small-molecule HuR ligands from two chemotypes (dicarboxylic acid and pyrrole scaffolds). These compounds revealed a previously unknown binding pocket in RRM3, whereas the bead-based setup provided an inherent assay for deorphanization. Based on an educated guess, we hypothesized and experimentally verified that ATP is a natural ligand for this site. Strategically selected HuR mutants mapped the ATP complexation to an evolutionary conserved, Me^{2+}-binding DxD motif ($D_{254}AD_{256}$) in RRM3. Our data further show that the functional relevance of the HuR–ATP interaction is associated with an RNA-modifying, terminal adenosyl transferase activity of HuR RRM3.

While the first low molecular weight inhibitors for HuR RRM1+2 have been described recently,[23] the structurally uncharacterized and biochemically problematic (i.e., low solubility and expression efficiency) RRM3 presents an unequally greater challenge for ligand identification. Yet, the availability of RRM3-targeted (tool) compounds is of high interest, as a critical role of this domain for mediating protein–protein interactions and post-translational modifications of HuR and its interplay with up- and downstream processes have become evident.[25,26,29,34,51,52] In such a situation, where no chemical starting point or structural information is available, affinity-based screening represents the method of choice to identify small-molecule ligands. However, the low solubility of full-length HuR and RRM3 presents a major obstacle to the application of widely used methods such as fragment-based screening or affinity chromatography (e.g., Speed Screen[53]), which require a considerably high concentration of protein and/or ligands. Moreover, due to the shallow, featureless sites that are often to be expected for protein–protein or dynamic interactions, the screening method also has to be capable of retrieving low-

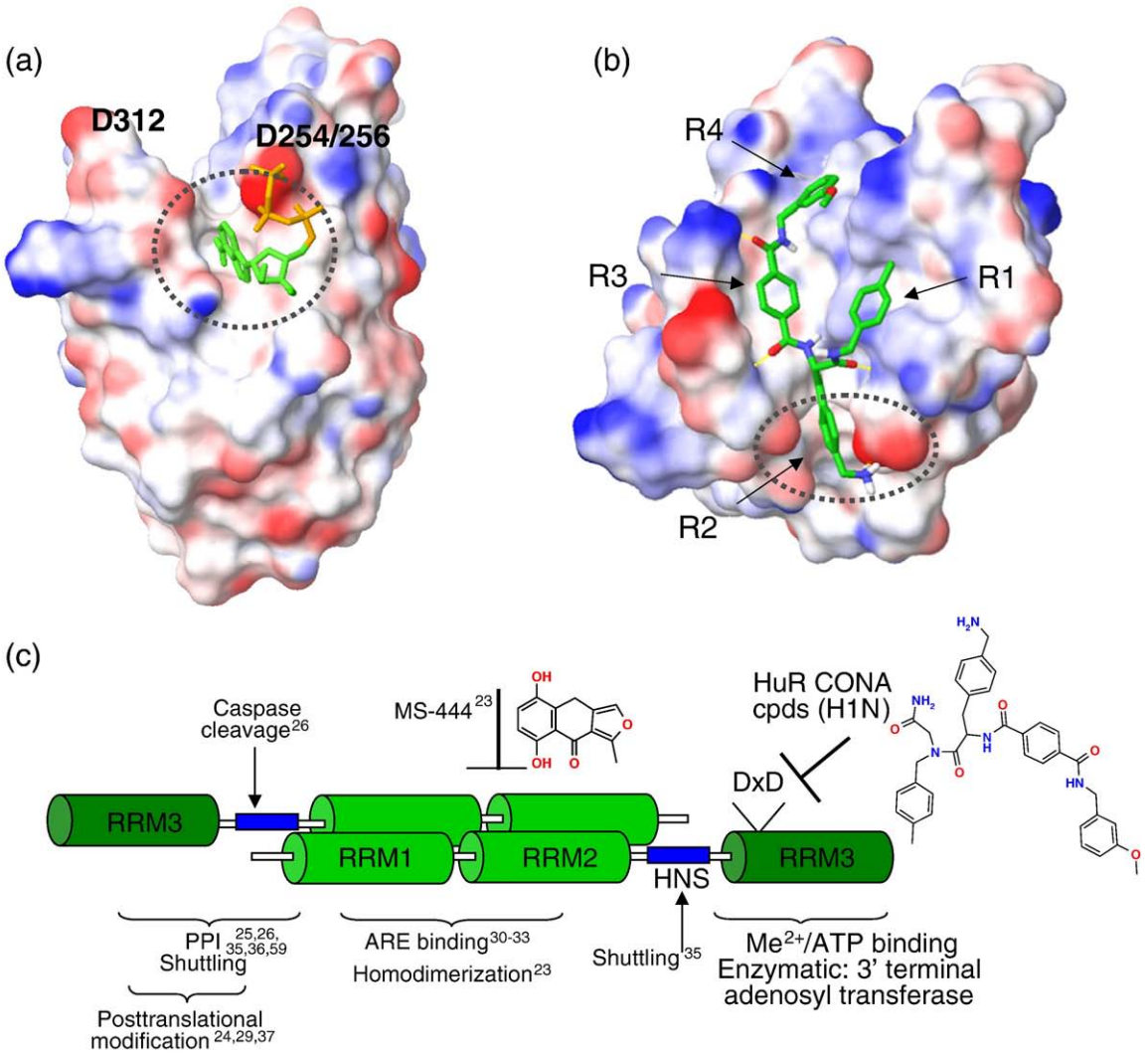

Fig. 7. Conservation of a DxD motif in RRM3 and global RRM3 structure prediction. (a) A homology model of HuR RRM3 illustrates the predicted protein surface, coloured by electrostatic potential (red, negative charges; blue, positive charges). Both $D_{254}xD_{256}$ and D_{312} are predicted to be surface exposed and in proximity of a positively charged, putative RNA binding groove. The hypothetical binding mode of ATP as predicted by docking (GLIDE 4.5), mediated via Mg^{2+} coordination by $D_{254}xD_{256}$ is shown. (b) Hypothetical binding mode of the dicarboxylic acid compound H1N, as predicted by docking. (c) HuR domain organization and functional annotation: schematic overview of current knowledge of HuR protein or small-molecule ligands and functional HuR activities, mapped to the corresponding RRM or hinge domains. HuR is functional as a high-affinity homodimer, mediated via a dimerization interface within RRM1+2.[23] Binding to the ARE RNA has been assigned to these tandem RRMs,[30–33] whereas each HuR monomer contacts a single-stranded NNUUNNUUU nonamer.[23,31] An interaction with protein ligands has been described for RRM1 (von Hippel–Lindau, VHL[9]) as well as for the hinge region and RRM3 (pp32,[25,26] APRIL,[25] SETα/β,[25] CARM-1,[37] protein kinase C delta,[24,29] caspases3 and 7[26]) and were shown to influence HuR mRNA binding or nucleocytoplasmic transport, respectively. A nuclear localization signal within the hinge region (HNS, HuR nuclear localization signal[35]) was shown to regulate the localization of HuR via interaction with adaptors for nuclear export [pp32,[25] APRIL,[25] or import (transportin-1 and -2,[36,47] importin α[48])]. In addition, the hinge region and RRM3 were also shown to be the primary sites for posttranslational modifications (methylation of Arg217 by CARM-1,[37] phosphorylation of Ser221 and Ser318 by protein kinase C delta[24,29]), which play a role mainly in nucleocytoplasmic trafficking.[34,35] A posttranslational phosphorylation of RRM1 was also reported and associated with modulation of HuR mRNA interaction (phosphorylation of Ser100 by Chk2[29]). In this study, we reveal an ATP-binding pocket centred around a Me^{2+}-binding DxD motif (Asp254, Asp256) in RRM3, and its involvement in an RNA-modifying 3′-terminal adenosyl transferase activity of the third HuR domain. The recently described caspase-mediated cleavage of HuR within the hinge region (Asp226)[26] might well serve to separate the newly identified enzymatic activity of RRM3 from the rest of the protein. Small-molecule HuR inhibitors, which have been described to date, comprise RRM1+2-targeted inhibitors of HuR homodimerization (MS-444, dehydromutactin, okicenone[23]) as well as ligands to the ATP-binding pocket in RRM3 (HuR CONA hits, described in this study).

affinity ligands. Due to the high local compound densities, bead-based screening allows both, dealing with low target concentrations and detecting low-affinity interactions.[54] CONA on-bead screening proved ideally suited to identifying low-affinity, yet specific RRM3 binders. Beyond that, the

quantitative nature of the technology together with the assets of on-bead detection led to the revelation of the so far unnoticed, micromolar-affinity (K_d) HuR ligand ATP.

To put these new findings into perspective, the current knowledge on HuR ligands described in this and previous studies is summarized in Fig. 7c. While RRM3 has been associated with protein–protein interactions and now with an ATP-binding and enzymatic function, it is still an RNA binding domain and therefore most probably also has a cognate RNA ligand. As the RRM3-targeted CONA compounds interfere with both ATP and ARE RNA binding, this suggests that also RRM3 forms contacts to the RNA, distant from the RRM1+2–NNUUNNUUU interaction. According to the data shown in Fig. 5, NNUUNNUUU is neither necessary nor required in HuR substrate selection for enzymatic modification by RRM3. This in turn indicates the existence of a separate RNA binding motif for the third HuR domain, which may or may not function *in cis* to NNUUNNUUU. The fact that the isolated RRM3 domain showed a significantly reduced enzymatic activity compared to the full-length protein suggests at least an indirect contribution of RRM1+2 and/or the hinge region to the reaction. The relation between RNA (substrate) recognition by RRM1/2 *versus* RRM3 and the enzymatic function of RRM3 becomes of specific interest if one considers the recently demonstrated caspase-mediated cleavage of HuR within the hinge region.[26] Such a protease-mediated segregation of the N- and C-terminal moieties might well serve as a regulatory mechanism involving an irreversible termination of HuR enzyme activity.

Resolving the detailed molecular mechanism of the enzymatic reaction and the implications for RNA regulation will now be the next scientific challenge in HuR research. In a first attempt, we tried to integrate the newly identified enzymatic activity into current classifications of RNA ribonucleotidyl transferases. The main features of RRM3 shared with other transferases are a conserved DxD motif and a third aspartate further downstream, which is also found in Pol-β type nucleotidyl transferases. Besides that however, RRM3 does not match the Pol-β type consensus motif (hG[GS]$x_{(7–13)}$Dh[DE]h). In addition, the active site in HuR (Fig. 7a) is predicted to be localized on the two loops at one end of the β-sheet, which is unprecedented among Pol-β transferases. Also, other features of this closest class of enzymes are lacking in RRM3. Therefore, based on structural features the integration of HuR into existing classifications of transferases is not obvious. We thus turned to a functional comparison with other 3′-terminal RNA-modifying enzymes. In line with template-independent transferases or polymerases,[45] HuR showed a low level of selectivity in binding to the four NTPs (with the exception of GTP), but a clear catalytic selectivity for one specific nucleotide (ATP). Also, the observed 3′-terminal RNA substrate modification occurred in the absence of an RNA template strand. Both of these observations argue against a template-dependent polymerase function of HuR. Also, a template-independent homopolymerization activity is unlikely because we observed neither a significant elongation of the RNA substrates after reaction nor an interaction of HuR with preformed poly(A) stretches (Supplementary Online Material). This is in contrast to previous reports of a poly(A)-binding activity of HuR RRM3,[30,55] which has remained widely accepted despite contradictory evidence in other studies.[56] Also, the lack of recognition of 3′-terminally polyadenylated substrates for the HuR enzyme (Fig. 5) is in conflict with a poly(A)-tailing function. In our *in vitro* assay, the number of incorporated adenosyl residues estimated from isotopic incorporation was around one or at most a few nucleotides per RNA molecule. Hence, the length of the 3′ modification might potentially be limited by the number of successive adenines tolerated in the RNA binding groove of RRM3. Alternatively, it can also not be excluded that HuR still functions as a (nonprocessive) homopolymerase, but that recycling for additional rounds of catalysis requires yet-to-be identified cofactors.

Altogether, this is the first demonstration of an enzymatic activity for an ELAV protein that sheds an entirely new light on the mode of action underlying HuR-controlled mRNA and/or microRNA regulation. While at this point we cannot rule out that *in vivo*, additional factors further modulate the actual enzymatic reaction (compare Fig. 6), a picture emerges where HuR functions as a 3′-terminal RNA-editing enzyme with an active role in maturation and metabolism of mRNA or microRNA targets. We believe that these findings set the stage for a new direction in HuR research, where the physiological context of an RNA modification by HuR will be a complex and challenging question. There are an intractable number of potential substrates of unknown RNA type, sequence, and length. The quest is further complicated by the herein demonstrated independence of previously established criteria for RNA recognition by RRM1+2. Also, studying a potential regulatory RNA modification by HuR in cells will require a signal that specifically probes this reaction. Alternatively, for characterizing the HuR enzyme in phenotypic assays, a potent RRM3 enzymatic inhibitor will be needed. The compounds described in this study will present valuable starting points to address these questions.

Methods

Preparation of recombinant proteins and RNA

Recombinant human full-length HuR (SwissProt accession no. Q15717) and HuR_{12} (aa 2–189) were prepared as described previously.[31] Site-directed mutagenesis was performed by PCR-driven overlap extension[57] using a plasmid containing WT full-length HuR[31] as template (for details, see Supplementary Online Material). All sequences were verified by DNA sequencing. The mutant proteins were expressed in *E. coli* ER2566 and purified following the same procedure as described for the WT protein.[31] The

preparation of HuR RRM3 (as fusion protein with mCherry) is described in the Supplementary Online Material. The quality of the proteins was controlled by reversed-phase HPLC (RP-HPLC) and SDS-PAGE analysis and verified a purity of >95% and a band at the expected size of 36 kDa, respectively. DNA templates for *in vitro* transcription of 3′ UTR fragments [IL-2, TNF-α, IL-1β, VEGF (vascular endothelial growth factor)] were amplified from cDNA from human peripheral mononuclear cells and RNA was generated by run-off transcription with T7 polymerase. CAT1 3′UTR fragments containing or missing the ARE were kindly provided by S. Ameres and prepared as described previously.[19] RNA sequences of up to 35 nucleotides were synthesized in-house or purchased from Microsynth (Switzerland). All sequences are detailed in the Supplementary Online Material. Total RNA and poly(A) RNA from mammalian cells (HEK293T cells, 5×10^6 cells each) were purified using commercially available kits (RNeasy and Oligotex mRNA kits, respectively, both from Qiagen).

Confocal Nanoscanning of one-bead–one-compound libraries on-bead

Protein labelling

Due to the high hydrophobicity of full-length HuR, standard fluorescence-labelling protocols with a variety of amino- or thiol-reactive dyes (Cy5, Cy3, Alexa488, Alexa647, TMR) led to a precipitation of the protein even at submicromolar concentrations. We therefore turned to a site-specific C-terminal derivatization using a homemade labelling and solubility-enhancing peptide combined with a purification tag (specified in Supplementary Online Material). Briefly, the peptide was composed of an N-terminal cystein, a lysine-conjugated Cy5 dye, a solubility-enhancing PEG (polyethylene glycol) linker, and a C-terminal His_6 tag. The peptide was coupled by native chemical ligation[58] to the C-terminal mercaptoethanesulfonic acid thioester on HuR, as generated by the IMPACT system (New England Biolabs). HuR_{12} was labelled following an analogous procedure. The labelled proteins were analyzed by RP-HPLC, SDS-PAGE analysis, CD spectroscopy and fluorescence correlation spectroscopy. To confirm a retained activity after labelling, the proteins were transfected into primary T cells by electroporation (Amaxa) to measure the effect on IL-2 expression (Supplementary Online Material).

CONA screen

On-bead libraries were synthesized on AIDA-loaded 90 -μm TentaGel beads from Rapp polymers by a split–mix–divide procedure essentially as described in Ref. 59. To assemble a master plate of 96 on-bead sublibraries, 1 mg of each resin (i.e., ~2000 beads) was suspended and sonicated in screening buffer [phosphate-buffered saline (PBS) pH 7.2, 0.2% (w/v) Pluronic F-127, 5 mM $MgCl_2$] and transferred into one well of a microtiter plate, resulting in a monolayer of beads at the well bottom. Fluorescently labelled HuR_{fl} or HuR_{12} was added at a concentration of 40 nM and incubated with the beads overnight at room temperature. The beads were scanned on a custombuilt confocal scanning microscope adapted for large-area scanning (PS02, Perkin Elmer Cellular Technologies, former Evotec Technologies). Scanning parameters were the following: resolution, 5 μm; speed, 8 mm s^{-1}; scanning height, 30 μm (autofocus controlled); excitation, 633-nm HeNe laser (5 μW), 670/40-nm band-pass filter; emission, 590-nm dichroic mirror, 690/40-nm band-pass filter; detection, fiber coupled APDs (EG&G). Scan images were analyzed by a proprietary software (BeadEval, Evotec Technologies). Hit beads were identified and ranked based on the fluorescence intensity of bound HuR at the bead surface (≤5-μm outer layer). The 46 top-ranked hit beads were isolated based on the x/y coordinates in the well using an integrated picking device that allowed the transfer of single beads by hydraulic dispensing (capillaries of 160 μm inside diameter) into individual glass vials. The compound was UV-cleaved from the resin in methanol, 1% (v/v) trifluoroacetic acid (120 min, 365 nm, 1070 μJ min^{-1}). The hit structure was elucidated by RP-μHPLC/MS and MS^2 analysis using the compound fragmentation pattern and the AIDA tag as a tracer. Resynthesis of the selected hit compounds and their analytical characterization is described in Supplementary Online Material.

On-bead binding and competition assay using HuR CONA hit compounds

To assay direct binding of HuR to bead-immobilized compounds, the resin was swollen in buffer [PBS, 0.2% (w/v) Pluronic F-127, 5 mM $MgCl_2$]. Aliquots of the bead suspension containing ~500 beads each were incubated with unlabelled HuR_{fl} or HuR_{12} at 200 nM for 120 min at room temperature under agitation, followed by antibody staining (primary antibody, mouse anti-HuR IgG, 19F12; detection antibody:,Alexa 647-conjugated goat anti-mouse IgG, Molecular Probes; both at 20 μg ml^{-1} and an incubation time of 60 min]. The resin was washed with assay buffer in between all steps. For competition experiments, the swollen resin was preincubated with the competitor (concentration as indicated for each data set) for 30 min prior to addition of HuR. After antibody staining, the samples were scanned by CONA in a 384-well glass-bottomed plate, as described above. Essentially the same procedure was followed to monitor HuR binding to bead-immobilized ATP (polyacrylamide beads, Novagen), but using the manufacturer's detergent in the assay buffer. On-bead binding was quantified by a software-based determination of the fluorescence ring intensities of all beads and averaged over the 100 beads centred around the geometric mean. Measurements of on-bead binding kinetics are described in the Supplementary Online Material.

HuR RNA binding assay

Binding of HuR_{12} and HuR_{fl} (WT and mutants) to 5′TMR-labelled RNA in the presence or absence of competitors (ATP, CONA compounds) was measured by confocal fluctuation spectroscopy (2D-FIDA) as described previously.[23]

HuR dimerization assay

Homodimerization of WT and mutant HuR_{fl} was monitored by Western blotting as described previously.[23] Additionally, a sandwich ELISA allowed the detection of HuR dimers by using capture (19F12 mouse anti-HuR, Clonegene; coated at 1 μg ml^{-1}) and detection antibodies (H-280 rabbit anti-HuR, Santa Cruz Biotechnology, at 0.5 μg ml^{-1}) that recognize a common epitope at the HuR N-terminus (detailed in Supplementary Online Material).

HuR ATP/GTP binding assay

HuR_{12} or HuR_{fl} (600 nM, WT and mutants) was preincubated with different concentrations (0–100 μM) of ATP-

Bodipy FL or GTP-Bodipy FL (Molecular Probes) for 60 min at room temperature in the presence or absence of competitors as specified. After capturing for 60 min to an antibody-coated ELISA plate (19F12 mouse anti-HuR, coated at 1 μg ml^{-1}), the plates were washed and HuR-complexed ATP or GTP was detected via the Bodipy FL fluorescence (excitation/emission filters: 485/20, 535/25; TECAN Ultra). Identical concentrations of ATP-Bodipy FL or GTP-Bodipy FL without HuR were used for background correction.

Homology modelling and docking

The template structures (PDB codes 1D8Z, 1PIT, 2CPZ, 2HYI, and 2SXL) were selected from a BLAST search of the HuR sequence (Q15717) against the PDB, followed by a multiple sequence alignment (ClustalW). For each of these templates, homology models were built with the Modeller software and relaxation and energy minimizations were performed with NAMD 2.5 (40 Å water sphere, 0.5 -ns molecular dynamics simulation time). A combined model was generated with the Modeller software, whereas the N-terminus was manually adjusted to the structure of 2HYI (due to problems with the positioning of the W_{244} residue), followed by a final energy minimization with NAMD 2.5.

The homology model structure of the HuR RRM3 domain was prepared for docking using the "Protein Preparation Wizard" Workflow in Maestro 8.0.314, whereas the C- and N-termini were virtually capped with *N*-methyl and *N*-acetyl groups, respectively. Mg^2 was manually positioned in the neighbourhood of the carboxylic acid group of D_{254} and the resulting structure was relaxed with a constrained minimization (Mg^2 unconstrained, positions of all other heavy atoms frozen; Maestro 8.0.314). Grids were centred around residues D_{312} and D_{254}, using a box size of 25 Å, to capture the entire RRM3 domain (Glide 4.5, default settings). Docking was done in standard precision mode. Flips of five- and six-membered rings were not allowed and non-planar conformations of amide bonds were penalized. 3D coordinates of ATP, H1N, or H2N used for docking were generated using LigPrep (Schroedinger, Maestro 8.0.314). A postdocking minimization was performed with the 20 top-ranked poses of the ligand.

ATP hydrolysis

α-^{33}P-labelled ATP (2 μCi, 330 nM) was incubated with calf intestinal phosphatase (5 U), HuR_{fl} (750 nM), HuR_{12} (750 nM) or *E. coli* poly(A) polymerase (4 U) for 120 min at 37 °C. Samples were separated by thin-layer chromatography on polyethyleneimine cellulose (0.1 mm, Cel 300 PEI, Machery&Nagel) in an eluent of 0.7 M KH_2PO_4 (pH 3.5) and analyzed by autoradiography.

Nucleotidyl transferase experiments

α-^{33}P-labelled ATP, GTP, CTP, or UTP (2 μCi, 330 nM) was incubated for between 30 and 120 min at 37 °C with full-length HuR, HuR_{12}, or HuR RRM3–mCherry (each at 750 nM) or PAP (4 U) in PBS containing 0.2% (w/v) Pluronic F-127, with RNA (1 μg of total RNA, individual RNA samples at 5 μM) and metal ions (10 mM $MgCl_2$, 1 mM $MnCl_2$) as specified. All samples were separated by thin-layer chromatography and visualized by autoradiography as described above. For PAGE experiments, IL-2 and IL-1β 3′UTR samples were *in vitro* polyadenylated with *E. coli* PAP (EpiCentre Biotech) with 1 mM ATP for 30 min at 37 °C. Alternatively, the RNA samples were 3′-terminally capped by conjugation to Cy3 hydrazide after oxidation of the 3′-terminal ribose.[60] After incubation with α-^{32}P-labelled ATP (2 μCi, 330 nM) and HuR_{12} or HuR_{fl} (both at 750 nM) for 15 h at 37 °C, the RNA samples were run on a 6% polyacrylamide/urea gel and visualized by ethidiumbromide staining or autoradiography.

Acknowledgements

The authors thank Rene Amstutz and Jan E. DeVries for continuous support, Stefan Ameres for providing CAT1 RNA, Rocco Angelo Falchetto for MS analysis support, Thomas Jung for his contributions to HuR activity tests, and Matthew Ross for native speaker support. N.M. thanks Imed Gallouzi and Witold Filipowicz for critical reading of the manuscript. This work was supported by a scholarship of the Austrian Academy of Sciences. The project was designed and coordinated by M.A., N.M., and M.H. RNA was prepared by N.M., J.S., and M.L. HuR_{12} and HuR_{fl} WT protein was prepared by N.M., HuR mutants were prepared by R.B. and R.M.B. HuR interaction studies were carried out by N.M. Peptide tags for C-terminal HuR labelling were synthesized by J.S., HuR labelling was performed by N.M. V.U. was responsible for the setup of confocal instruments. CONA experiments were performed by M.H. and N. M. CONA on-bead libraries were designed by H.G. and M.A.; structures of hit compounds were elucidated by H.G. ATP experiments were done by N.M., M.H., and J.S. The HuR homodimerization ELISA assay was established by R,B. The HuR RRM3 homology model was generated by R.M.B. and A. W. and used for docking experiments by T.S. N.M., M. H., and M.A. wrote the manuscript. All authors discussed the results and commented on the manuscript. All experimental work reported in this manuscript was done at the Novartis Institutes for Biomedical Research – Vienna.

Supplementary Data

Supplementary data associated with this article can be found, in the online version, at doi:10.1016/j.jmb.2008.12.020

References

1. Chen, C. Y. & Shyu, A. B. (1995). AU-rich elements: characterization and importance in mRNA degradation. *Trends Biochem. Sci.* **20**, 465–470.
2. Bakheet, T., Williams, B. R. & Khabar, K. S. (2006). ARED 3.0: the large and diverse AU-rich transcriptome. *Nucleic Acids Res.* **34**, D111–D114.
3. Abdelmohsen, K., Lal, A., Kim, H. H. & Gorospe, M. (2007). Posttranscriptional orchestration of an anti-apoptotic program by HuR. *Cell Cycle*, **6**, 1288–1292.
4. López de Silanes, I., Lal, A. & Gorospe, M. (2005). HuR—posttranscriptional paths to malignancy. *RNA Biol.* **2**, e11–e13.

5. Lopez DeSilanes, I., Fan, J., Yang, X., Zonderman, A. B., Potapova, O., Pizer, E. S. & Gorospe, M. (2003). Role of the RNA-binding protein HuR in colon carcinogenesis. *Oncogene*, **22**, 7146–7154.
6. Mrena, J., Wiksten, J. P., Thiel, A., Kokkola, A., Pohjola, L., Lundin, J. *et al.* (2005). Cyclooxygenase-2 is an independent prognostic factor in gastric cancer and its expression is regulated by the messenger RNA stability factor HuR. *Clin. Cancer Res.* **11**, 7362–7368.
7. Erkinheimo, T. L., Lassus, H., Sivula, A., Sengupta, S., Furneaux, H., Hla, T. *et al.* (2003). Cytoplasmic HuR expression correlates with poor outcome and with cyclooxygenase 2 expression in serous ovarian carcinoma. *Cancer Res.* **63**, 7591–7594.
8. Erkinheimo, T. L., Sivula, A., Lassus, H., Heinonen, M., Furneaux, H., Haglund, C. *et al.* (2005). Cytoplasmic HuR expression correlates with epithelial cancer cell but not with stromal cell cyclooxygenase-2 expression in mucinous ovarian carcinoma. *Gynecol. Oncol.* **99**, 14–19.
9. Datta, K., Mondal, S., Sinha, S., Li, J., Wang, E., Knebelmann, B. *et al.* (2005). Role of elongin-binding domain of von Hippel–Lindau gene product on HuR-mediated VPF/VEGF mRNA stability in renal cell carcinoma. *Oncogene*, **24**, 7850–7858.
10. Heinonen, M., Bono, P., Narko, K., Chang, S. H., Lundin, J., Joensuu, H. *et al.* (2005). Cytoplasmic HuR expression is a prognostic factor in invasive ductal breast carcinoma. *Cancer Res.* **65**, 2157–2161.
11. Heinonen, M., Fagerholm, R., Aaltonen, K., Kilpivaara, O., Aittomaki, K., Blomqvist, C. *et al.* (2007). Prognostic role of HuR in hereditary breast cancer. *Clin. Cancer Res.* **13**, 6959–6963.
12. Carlsson, A. & Schwartz, S. (2000). Inhibitory activity of the human papillomavirus type 1 AU-rich element correlates inversely with the levels of the elav-like HuR protein in the cell cytoplasm. *Arch. Virol.* **145**, 491–503.
13. Niesporek, S., Kristiansen, G., Thoma, A., Weichert, W., Noske, A., Buckendahl, A. C. *et al.* (2008). Expression of the ELAV-like protein HuR in human prostate carcinoma is an indicator of disease relapse and linked to COX-2 expression. *Int. J. Oncol.* **32**, 341–347.
14. Nabors, L. B., Suswam, E., Huang, Y., Yang, X., Johnson, M. J. & King, P. H. (2003). Tumor necrosis factor alpha induces angiogenic factor up-regulation in malignant glioma cells: a role for RNA stabilization and HuR. *Cancer Res.* **63**, 4181–4187.
15. Denkert, C., Koch, I., von, K. N., Noske, A., Niesporek, S., Dietel, M. & Weichert, W. (2006). Expression of the ELAV-like protein HuR in human colon cancer: association with tumor stage and cyclooxygenase-2. *Mod. Pathol.* **19**, 1261–1269.
16. Eberhardt, W., Doller, A., Akool, E. & Pfeilschifter, J. (2007). Modulation of mRNA stability as a novel therapeutic approach. *Pharmacol. Ther.* **114**, 56–73.
17. Brennan, C. M. & Steitz, J. A. (2001). HuR and mRNA stability. *Cell. Mol. Life Sci.* **58**, 266–277.
18. von Roretz, C. & Gallouzi, I.-E. (2008). Decoding ARE-mediated decay: is microRNA part of the equation? *J. Cell Biol.* **181**, 189–194.
19. Bhattacharyya, S. N., Habermacher, R., Martine, U., Closs, E. I. & Filipowicz, W. (2006). Relief of microRNA-mediated translational repression in human cells subjected to stress. *Cell*, **125**, 1111–1124.
20. Weiss, W. A., Taylor, S. S. & Shokat, K. M. (2007). Recognizing and exploiting differences between RNAi and small-molecule inhibitors. *Nat. Chem. Biol.* **3**, 739–744.
21. Eggert, U. S., Field, C. M. & Mitchison, T. J. (2006). Small molecules in an RNAi world. *Mol. Biosyst.* **2**, 93–96.
22. Fitzgerald, K. (2005). RNAi versus small molecules: different mechanisms and specificities can lead to different outcomes. *Curr. Opin. Drug Discov. Dev.* **8**, 557–566.
23. Meisner, N. C., Hintersteiner, M., Mueller, K., Bauer, R., Seifert, J. M., Naegeli, H. U. *et al.* (2007). Identification and mechanistic characterization of low-molecular-weight inhibitors for HuR. *Nat. Chem. Biol.* **3**, 508–515.
24. Doller, A., Huwiler, A., Mueller, R., Radeke, H. H., Pfeilschifter, J. & Eberhardt, W. (2008). Protein kinase C alpha-dependent phosphorylation of the mRNA-stabilizing factor HuR: implications for posttranscriptional regulation of cyclooxygenase-2. *Mol. Biol. Cell*, **18**, 2137–2148.
25. Brennan, C. M., Gallouzi, I.-E. & Steitz, J. A. (2000). Protein ligands to HuR modulate its interaction with target mRNAs in vivo. *RNA*, **7**, 1–13.
26. Mazroui, R., Di, M. S., Clair, E., von, R. C., Tenenbaum, S. A., Keene, J. D. *et al.* (2008). Caspase-mediated cleavage of HuR in the cytoplasm contributes to pp32/PHAP-I regulation of apoptosis. *J. Cell Biol.* **180**, 113–127.
27. David, P. S., Tanveer, R. & Port, J. D. (2007). FRET-detectable interactions between the ARE binding proteins, HuR and p37AUF1. *RNA*, **13**, 1453–1468.
28. Van Der, G. K. & Gallouzi, I. E. (2007). Involvement of transportin 2-mediated HuR import in muscle cell differentiation. *Mol. Biol. Cell.* **18**, 2619–2629.
29. Abdelmohsen, K., Pullmann, R., Jr., Lal, A., Kim, H. H., Galban, S., Yang, X. *et al.* (2007). Phosphorylation of HuR by Chk2 regulates SIRT1 expression. *Mol. Cell*, **25**, 543–557.
30. Ma, W.-J., Chung, S. & Furneaux, H. (1997). The ELAV-like proteins bind to AU-rich elements and to the poly(A) tail of mRNA. *Nucleic Acids Res.* **25**, 3564–3569.
31. Meisner, N. C., Hackermuller, J., Uhl, V., Aszodi, A., Jaritz, M. & Auer, M. (2004). mRNA openers and closers: modulating AU-rich element-controlled mRNA stability by a molecular switch in mRNA secondary structure. *Chembiochem*, **5**, 1432–1447.
32. Chung, S., Jiang, L., Cheng, S. & Furneaux, H. (1996). Purification and properties of HuD, a neuronal RNA-binding protein. *J. Biol. Chem.* **271**, 11518–11524.
33. Sakai, K., Kitagawa, Y. & Hirose, G. (1999). Analysis of the RNA recognition motifs of human neuronal ELAV-like proteins in binding to a cytokine mRNA. *Biochem. Biophys. Res. Commun.* **256**, 263–268.
34. Gallouzi, I. E. & Steitz, J. A. (2001). Delineation of mRNA export pathways by the use of cell-permeable peptides. *Science*, **294**, 1895–1901.
35. Fan, X. C. & Steitz, J. A. (1998). HNS, a nuclear–cytoplasmic shuttling sequence in HuR. *Proc. Natl Acad. Sci. USA*, **95**, 15293–15298.
36. Guttinger, S., Muhlhausser, P., Koller-Eichhorn, R., Brennecke, J. & Kutay, U. (2004). From the cover: transportin2 functions as importin and mediates nuclear import of HuR. *Proc. Natl Acad. Sci. USA*, **101**, 2918–2923.
37. Li, H., Park, S., Kilburn, B., Jelinek, M. A., Henschen-Edman, A., Aswad, D. W. *et al.* (2002). Lipopolysaccharide-induced methylation of HuR, an mRNA-stabilizing protein, by CARM1. *J. Biol. Chem.* **277**, 44623–44630.

38. Peng, L., Liu, R., Marik, J., Wang, X., Takada, Y. & Lam, K. S. (2006). Combinatorial chemistry identifies high-affinity peptidomimetics against alpha4beta1 integrin for in vivo tumor imaging. *Nat. Chem. Biol.* **2**, 381–389.
39. Lam, K. S., Liu, R., Miyamoto, S., Lehman, A. L. & Tuscano, J. M. (2003). Applications of one-bead one-compound combinatorial libraries and chemical microarrays in signal transduction research. *Acc. Chem. Res.* **36**, 370–377.
40. Auer, M. & Gstach, H. (2001). Fluorescent dyes for solid phase and solution phase screening.US Patent US6207831.
41. Meisner, N. C., Hintersteiner, M., Uhl, V., Weidemann, T., Schmied, M., Gstach, H. & Auer, M. (2004). The chemical hunt for the identification of drugable targets. *Curr. Opin. Chem. Biol.* **8**, 424–431.
42. Unligil, U. M. & Rini, J. M. (2000). Glycosyltransferase structure and mechanism. *Curr. Opin. Struct. Biol.* **10**, 510–517.
43. Yue, D., Weiner, A. M. & Maizels, N. (1998). The CCA-adding enzyme has a single active site. *J. Biol. Chem.* **273**, 29693–29700.
44. Martin, G. & Keller, W. (1996). Mutational analysis of mammalian poly(A) polymerase identifies a region for primer binding and catalytic domain, homologous to the family X polymerases, and to other nucleotidyltransferases. *EMBO J.* **15**, 2593–2603.
45. Martin, G. & Keller, W. (2007). RNA-specific ribonucleotidyl transferases. *RNA*, **13**, 1834–1849.
46. Aravind, L. & Koonin, E. V. (1999). DNA polymerase beta-like nucleotidyltransferase superfamily: identification of three new families, classification and evolutionary history. *Nucleic Acids Res.* **27**, 1609–1618.
47. Rebane, A., Aab, A. & Steitz, J. A. (2004). Transportins 1 and 2 are redundant nuclear import factors for hnRNP A1 and HuR. *RNA*, **10**, 590–599.
48. Wang, W., Yang, X., Kawai, T., Lopez, D. S. I., Mazan-Mamczarz, K., Chen, P. *et al.* (2004). AMPK-regulated phosphorylation and acetylation of importin a1: involvement in the nuclear import of RNA-binding protein HuR. *J. Biol. Chem.* **279**, 48376–48388.
49. Wang, X. & Tanaka Hall, T. M. (2001). Structural basis for recognition of AU-rich element RNA by the HuD protein. *Nat. Struct. Biol.* **8**, 141–145.
50. Yarovinsky, T. O., Butler, N. S., Monick, M. M. & Hunninghake, G. W. (2006). Early Exposure to IL-4 stabilizes IL-4 mRNA in CD4 T cells via RNA-binding protein HuR. *J. Immunol.* **177**, 4426–4435.
51. Izquierdo, J. M. (2008). Hu antigen R (HuR) functions as an alternative pre-mRNA splicing regulator of Fas apoptosis-promoting receptor on exon definition. *J. Biol. Chem.* **283**, 3299–3307.
52. Toba, G. & White, K. (2008). The third RNA recognition motif of *Drosophila* ELAV protein has a role in multimerization. *Nucleic Acids Res.* **36**, 1390–1399.
53. Zehender, H., Le, G. F., Lehmann, N., Filipuzzi, I. & Mayr, L. M. (2004). SpeedScreen: the "missing link" between genomics and lead discovery. *J. Biomol. Screen.* **9**, 498–505.
54. Ying, L., Liu, R., Zhang, J., Lam, K., Lebrilla, C. B. & Gervay-Hague, J. (2005). A topologically segregated one-bead–one-compound combinatorial glycopeptide library for identification of lectin ligands. *J. Comb. Chem.* **7**, 372–384.
55. Abe, R., Sakashita, E., Yamamoto, K. & Sakamoto, H. (1996). Two different RNA binding activities for the AU-rich element and the poly(A) sequence of the mouse neuronal protein HuC. *Nucleic Acids Res.* **24**, 4895–4901.
56. Gao, F. B. & Keene, J. D. (1996). Hel-N1/Hel-N2 proteins are bound to poly(A) mRNA in granular RNP structures and are implicated in neuronal differentiation. *J. Cell Sci.* **109**, 579–589.
57. Heckman, K. L. & Pease, L. R. (2007). Gene splicing and mutagenesis by PCR-driven overlap extension. *Nat. Protoc.* **2**, 924–932.
58. Dawson, P. E., Muir, T. W., Clark-Lewis, I. & Kent, S. B. (1994). Synthesis of proteins by native chemical ligation. *Science*, **266**, 776–779.
59. Gstach, H. (2002). Tagging compounds and process for use in decoding and physical property modification of AIDA-based (i.e., fluorescent 1,3-diaryl-1*H*-indazole dye-based) combinatorial libraries. Patent No WO0236575.
60. Qin, P. Z. & Pyle, A. M. (1999). Site-specific labeling of RNA with fluorophores and other structural probes. *Methods*, **18**, 60–70.